Energy 194 (2020) 116862

Contents lists available at ScienceDirect

Energy

journal homepage: www.elsevier.com/locate/energy

Biosyngas-fueled platinum reactor applied in micro combined heat and power system with a thermophotovoltaic array and stirling engine

Wen-Lih Chen [a], Chao-Wei Huang [b], Yueh-Heng Li [a, *], Chien-Chun Kao [a], Huynh Thanh Cong [c]

[a] Department of Aeronautics and Astronautics, National Cheng Kung University, Tainan, 701, Taiwan, ROC
[b] Department of Department of Chemical and Materials Engineering, National Kaohsiung University of Science and Technology, Kaohsiung, 807, Taiwan, ROC
[c] VNU-HCM Key-lab for Internal Combustion Engine, Ho Chi Minh City University of Technology, Vietnam National University, Ho Chi Minh City, Viet Nam

ARTICLE INFO

Article history:
Received 9 October 2019
Received in revised form
20 December 2019
Accepted 26 December 2019
Available online 30 December 2019

Keywords:
Micro heat and power system
Combustion
Stirling engine
Thermophotovoltaic
Bio-syngas

ABSTRACT

Currently, alternative fuels, derived from biomass and urban maximize the overall power output, have been increasingly attracting more attention in the industrial and residential sectors. Micro-combined heat and power (CHP) systems with high energy efficiency have been developed, particularly for the use in remote and rural areas. This study used a micro-CHP system, with a combustion-driven thermophotovoltaic (TPV) cell array and a Stirling engine-driven power system, within which methane and bio-syngas fuels were deployed strategically. This micro-CHP system harvests energy generated through thermal radiation from the reactor surface and harvests thermal energy from hot flue gas. Eventually, the micro-CHP prototype was proven that all energies are converted to electricity, and hot water can be simultaneously supplied. High incandescent surface and high-temperature flue gas of platinum reactor provide the thermal sources for TPV cell array and Stirling engine. The overall efficiency of the micro-CHP system was 35.0% for 50%H_2+50%CO, and the generated power included 2.7, 3.5, and 272.1 W from the Stirling engine-driven power system, GaSb TPV cell array, and hot water supply system, respectively. The systematic performance of the micro-CHP system, the combustion features, radiation efficiency, fuel conversion rate, total electricity output, and corresponding overall efficiencies were examined thoroughly.

1. Introduction

Combined heat and power (CHP) systems are mainly built on the integration of a combined heat and power module. CHP systems are used as part of distributed generation (DG), primarily because they conserve energy, exhibit high energy efficiency, have low carbon dioxide emissions, and present other environmental benefits [1]. These systems adopt cascaded energy use to provide both heat and electricity. Moreover, they can be connected to a power grid, and off-grid CHP systems can improve energy efficiency by using waste heat directly during production. These systems lead to higher global efficiency than do the stand-alone power systems used in large power plants. CHP systems also allow primary energy conservation and emission reduction and enhance supply network reliability [2,3].

Micro-CHP can produce decentralized heat and electricity, which can be connected to a low-voltage grid [4]. DG with green energy can be a practical solution for achieving carbon abatement and increasing supply security [5]. In addition, distributed green energy generation can provide sustainable, reliable, and affordable energy for rural regions where is a lack of power and electrical grid infrastructure [6]. Diesel generators are the most commonly used power-isolated microgrids because of relatively-inexpensive installment cost, sophisticated technique, and high maneuverability to meet variable grid demand. However, diesel oil is costly, particularly in remote locations. Specifically, in such areas, electricity generation costs are high, and their emissions are harmful to the inhabitants. The use of generators that use renewable energy

* Corresponding author.
E-mail address: yueheng@mail.ncku.edu.tw (Y.-H. Li).

https://doi.org/10.1016/j.energy.2019.116862
0360-5442/

sources can provide or substitute fossil fuel-based electricity generation, thus alleviating or even eliminating the aforementioned disadvantages.

Bianchi et al. [7] reported an efficient method for solving the micro-CHP problem in the dwelling region. The authors reported a micro-CHP unit comprising a CHP prime mover, subsidiary boiler, and thermal storage unit. The electricity yielded by this unit can be either depleted on-site or converged into the power grid. Buragohain et al. [8] ascertained the feasibility of biomass gasification applied in decentralized power generation. Biomass-to-energy systems are regarded as a practical and feasible alternative for downsized and decentralized CHP [9]. Therefore, it can overcome the complexities of fuel supply logistics and inventory management in large-scale units [10]. In order to reduce transport costs, it is recommended to use locally available biomass for feeding small-scale biomass CHP systems to supply the generated heat and electricity to the nearby dwelling community. Compared to large-scale systems, small-scale systems are not always capable of satisfying the heat demand of local users [11,12]. Montuori et al. [13] simulated a microgrid, evaluated its economic performance by using a heuristic dispatch strategy, and concluded that biomass gasification is considerably more convenient than conventional energy supplied by a diesel generator. Ho et al. [14] introduced a design method for a biomass-based microgrid and optimized generator capacity in terms of weather variation and biomass availability. Zabaniotou et al. [15] presented the merit of a small-scale CHP system by conducting a chemical equilibrium model analysis. Their experimental results revealed that the system can subside biomass transportation costs and offer heat and power where and when necessary. Farhad et al. [16] investigated three layouts of SOFC micro-CHP systems proposed for dwelling applications. The results indicated that the overall electrical efficiency of the three tested layouts spanned from 33.9% to 42.4%. Regarding biogas application, Zeng et al. [17] studied the use of biogas-fueled flame fuel cell units, incorporating a two-layer porous medium burner and a microtubular SOFC, in micro-CHP applications. Chen et al. developed a biofuel CHP system with hybrid electrical energy storage (HES), leading to an overall energy efficiency increase to 63.10% [18]. Furthermore, the dynamic programming optimization was applied to a biofuel micro CHP-HES system, and the system efficiency was improved by 26.7% with the dynamic programming and decision tree strategy [19].

Biomass is regarded as a crucial and potential renewable energy resource [20]. The present biomass energy generation system can convert biomass into accessible energy [21,22]. However, the system must be improved in terms of the thermodynamic efficiency; system technology; emission level; and influence on water, food, and the environment. The syngas derived from biomass gasification system mainly comprises hydrogen (H_2), carbon monoxide (CO), and methane (CH_4) [23,24]. Furthermore, syngas can be synthesized to liquid hydrocarbon, which can be the fuels for combustion or a fuel cell. Syngas also can be directly used for combustion in conventional engines and gas turbines; this combustion is more efficient than direct feedstock combustion because syngas is combustible at high temperatures. In the spark-ignition engine, syngas use leads to lower CO, NO_x, and SO_2 emissions than does commercial natural gas use. Thus, the commercial natural gas engine can be coupled to syngas fed directly from a gasifier. Kohsri et al. [25] designed a hybrid syngas–solar photovoltaic (PV)–battery power system in Thailand. Different fuels, such as syngas, were combined to form a hybrid system, including rechargeable batteries. The maximum efficiency of the modified gas engine was 28.2%. Although the heating value of syngas (4.03 MJ/m^3) is considerably lower than that of natural gas (36 MJ/m^3), several micro-combustor and power generation applications [26,27] that only use syngas alone or with blended fuels have been established or are being studied [28,29]. Thus, in this study, we developed a novel power generation method, which facilitates syngas combustion to convert chemical energy resource into electricity, using a PV cell, particularly for deployment in rural and remote areas.

Although biomass is a plausible solution for developing renewable energy microgrids in rural areas, the variation in biomass feedstock is an inevitable challenge that should be considered when designing a reliable and stable micro-CHP system. The consistency of biofuel properties can be improved by conducting thermal degradation of various biomass feedstocks [30,31]; thus, the constituents of the resulting bio-syngas would differ. Designing a fuel-flexible combustor is presumably crucial for micro-CHP. Based on our previous studies [32,33], the catalytic combustion of the methane-air mixture can be sustained inside a micro-combustor by conducting catalytic combustion of the hydrogen-air mixture. Several researchers have proposed that CH_4 can be sustained inside a microreactor with [34,35] or without [36,37] the use of platinum when H_2 is added. H_2 addition promotes the catalytic combustion of CH_4 compared with the addition of platinum; however, the presence of CO can deteriorate the catalytic CH_4 combustion by contaminating the active catalyst surface, because compared with methane, CO has an inherently high sticking coefficient for the platinum surface. Li et al. [38] designed segmented catalytic interlacing with cavities that can reduce CO contamination on the platinum surface. With an increase in CO addition, H_2 tends to approach total conversion at higher temperatures. By contrast, a low amount of H_2 can promote catalytic CO oxidation, which can be oriented from the enhancement of the carboxyl pathway. Hydroxyl groups will react with CO adsorbed on the platinum surface, resulting in the formation of carbon dioxide. The additional kinetic interaction of H_2 and CO on the platinum surface was investigated by Mantzaras [39,40]. Their experimental results were in agreement with their numerical results; this can firmly explain the detailed reactions occurring between the oxidation of CO and H_2 for the promotion and inhibition reactions. By contrast, the quenching distance of CH_4 is considerably higher than that of H_2, which increases the difficulty in igniting within a small region. The numerical results showed that when H_2 or CO was premixed, the combustion of CH_4 on the platinum surface could be sustained within a specific mixing range. Li et al. [38] simulated a catalyst segmentation method with cavities to investigate the interaction among H_2, CO, and CH_4. Their results revealed that a heterogeneous reaction in the previous catalyst segment generates reactive radicals and induce exothermicity. Moreover, CH_4 can be conversed completely in a short distance with blended CO or H_2. Unlike the competition found in the conventional catalyst reactor, the processes of multifuel catalytic combustion are related to mutually assisted coupling between heterogeneous and homogeneous reactions.

The current micro-CHP system comprises a thermophotovoltaic (TPV) system and Stirling engine for power generation. The TPV system can straightly convert heat into electrical energy through a PV array, which is responsible for converting photons into electricity. A micro-TPV system, with a size of 0.113 cm^3, was developed in Singapore in 2002 [41]. As the system did not have any moving components, it could be comprehensively employed in commercial electronics, rather than conventional cells. In 2003, Nielsen et al. [42] proposed a micro-TPV system with a high surface area-to-volume ratio for achieving high power density. Although the power output and efficiency of the system were relatively low, they demonstrated the potential for further improvement in device operation, particularly that pertaining to basic modifications. The output power of the micro-TPV system increases while the package size decreases—the most notable finding among the micro-TPV

system studies [43,44].

Although the TPV system is a clean method of producing power, where energy is converted from photons to electricity, a considerable amount of heat is exhausted at the end of the combustion. This wasted energy can be reused by other thermal or external heat engines. A Stirling engine can produce mechanical work when it receives thermal energy from the heating chamber [45]. By combining the TPV system with a Stirling engine unit, higher total efficiency can be obtained.

A study indicated that H_2 and CH_4 can be sustained in the micro platinum tubular combustor [46]. The simulation results implied that the presence of a perforated gap can provide a space zone with lower velocity flow, which will slow down the flow velocity in localized spaces; this gap also served as a channel for trade and collection of the fuels and radicals between both two sides. Despite the inherently weak coupling in hybrid heterogeneous and homogeneous system for methane, it can efficiently induce methane catalytic combustion sustained in a small space. Accordingly, a micro platinum tubular combustor is an appropriate candidate to mitigate fuel variability and flame instability. Different ratios of H_2 and CO, which represent different compositions of syngas because of its production, were tested in the micro-combustor. The combustor phenomenon and operational characteristics of the micro-combustor system were determined by observing the flame behavior and measuring the luminous light intensity of the combustor. To verify the concept of the bio-syngas combustion–driven micro-CHP system, a thermophotovoltaic cell array, and a Stirling engine were integrated with a micro-combustor system fueled with bio-syngas. The GaSb TPV array, coaxially mounted with the micro-combustor, was used to convert the luminous light from the combustion surface to electricity. In the meantime, the Stirling engine, with a power generator, was connected on top of the micro-TPV system, and the engine was operated using the flue gas of the micro-combustor, with the water tank being used to store thermal energy for hot water supply. Furthermore, the power performance and overall efficiency of bio-syngas combustion–driven micro-CHP were assessed with regard to various hydrogen-to-carbon monoxide ratios. The final task of developing a micro-CHP system is to deploy and integrate the unit into a small grid and then reuse the waste heat from the combustion system to maximize the power output.

2. Experimental setup

2.1. Microscale combustor and measurement system

A platinum tubular micro-combustor was used for cogenerating incandescent radiation and high-temperature exhaust gas for the CHP system. To mitigate the fuel variability of the bio-syngas supply system and sustain a flamelet in a small space, a platinum reactor was used for inducing the catalytic combustion and achieving high fuel conversion. Studies have reported that the presence of H_2 can facilitate the onset of catalytic combustion of CO/H_2 syngas [38] and induce methane catalytic combustion in the parallel chamber by providing heat and radicals from CO/H_2 catalytic combustion [45]. The microscale combustion system constitutes a platinum tubular reactor (5.3 [inner diameter (ID)] × 6 [outer diameter (OD)] × 40 mm [length (L)] mm^3) and a quartz tube [8 (ID) × 10 (OD) × 70 (L) mm^3]. The platinum tube includes eight perforations with a diameter of 1 mm. These perforations are equidistantly placed at 5 mm from the bottom of the tube. The platinum tube and a stainless-steel tube [4 (ID) × 5.3 (OD) mm^2] are mounted together by a flange. In the connection section, the flange presents a backward-facing step (L: 5 mm). The quartz tube was fabricated to encompass the platinum tube, and the transparency of the quartz tube aids incandescent emission from the platinum tubular reactor passing and reaching to a thermophotovoltaic array. In addition, the quartz tube can direct high-temperature flue gas to the hot side of the Stirling engine. Fig. 1 shows a schematic of the microscale combustion system.

H_2, CO, and air were fueled to simulate various bio-syngas compositions for the inner combustion chamber, and CH_4-air was fueled to simulate the natural gas supply system for the outer combustion chamber. H_2, CO, CH_4, and air from pressurized bottles were measured by digital mass flowmeters (Brooks 5850E). The H_2 content of syngas varied from 90% to 10%, and accordingly, the resulting CO content of syngas varied from 10% to 90%. By contrast, the CH_4–air mixture for the outer combustion chamber and the flow velocity were fixed at the stoichiometric condition and 5 m/s, respectively. A digital camera (Nikon D80) captured the combustion characteristics of the micro-combustor under various fuel-air conditions. The aperture and the exposure time were set at f5.6 and 4000^{-1}s, respectively, for all photographs. The outlet of the experimental apparatus is displayed in Fig. 2. The wall temperature of platinum combustor was measured using an infrared thermal imaging camera (AVIO, Japan, model TVS-200EX Series) with 2% uncertainty. Gas chromatography was used for analyzing the chemical composition of the exhausted gas and calculating its combustion efficiency, and this flue gas was collected downstream of the quartz tube by using an elongated needle and then stored in a 1-L sampling bag. The irradiance of the micro-combustor was measured using a magnesium oxide-coated integrating sphere with

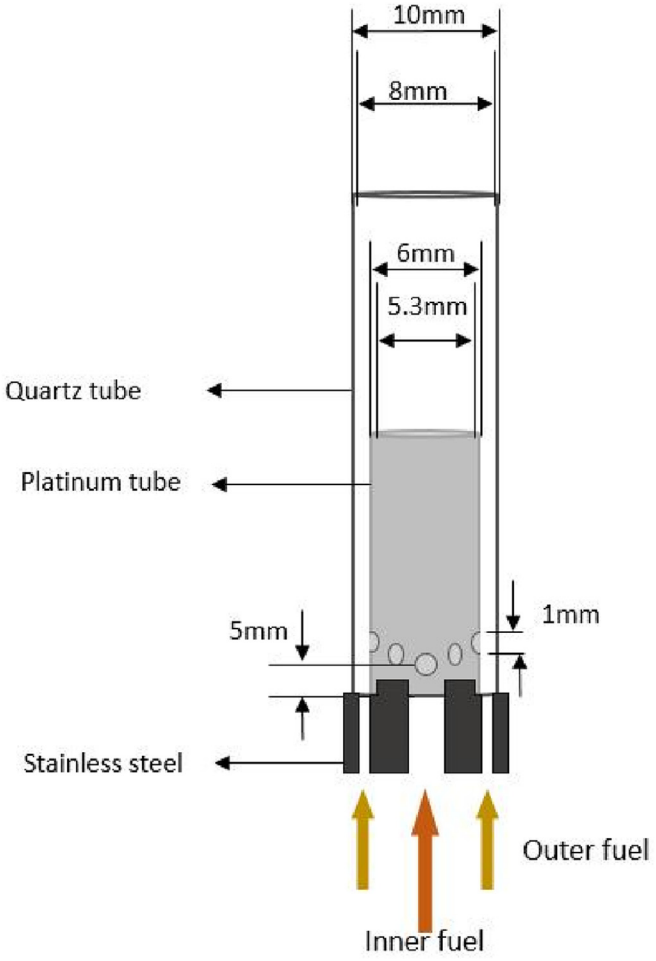

Fig. 1. Microscale combustion system.

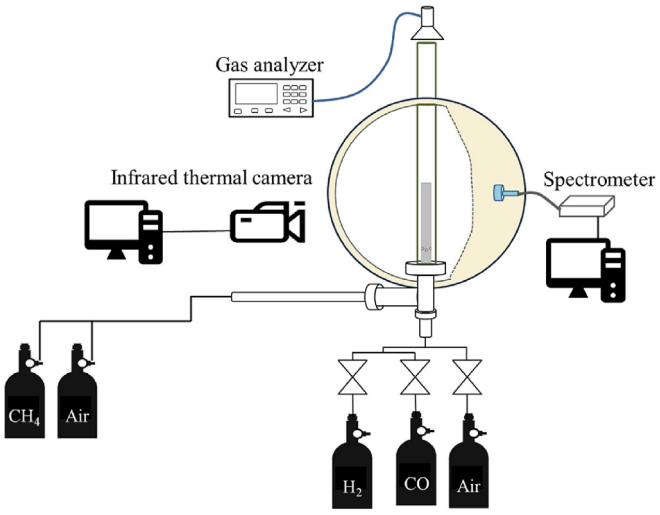

Fig. 2. Experimental apparatus and the corresponding measurement system.

a 15-cm diameter. The coating thickness of the integrating sphere is from 5 mm to 6 mm thick. When the irradiance measurement was conducted, the platinum combustor was assembled installed which was located in the center of the integrating sphere; and the emitted radiation from the surface of platinum combustor could scatter homogeneously onto its inner surface of the integrating sphere. A spectrometer (Ocean optic Inc., FL, USA) with a spectral wavelength of 200–1050 nm was linked to the integrating sphere to receive the radiation flux. The total irradiation was obtained by multiplying the radiation flux and the surface area of the platinum combustor. The overall radiant efficiency of the platinum micro-combustor is equivalent to the ratio of measured total irradiation from the emitting surface of the platinum combustor to the overall energy input of H_2/CO/CH_4 fuels. In order to evaluate the output power of the micro platinum combustion system, a PV cell array (Crystal Company) was placed such that it surrounded the reactor.

2.2. Thermophotovoltaic cell array

The emitting radiation performed the maximal spectrum intensity between 1100 nm and 1400 nm [45]. Thus, rather than silicon-based PV cells, a GaSb cell (JX Crystal, WA, USA), the absorption spectrum of which is 400–1800 nm, was used for energy conversion. Besides, the micro-combustor system encompassed a PV cell array, comprising single 2 × 12 GaSb cells. The PV cell array shows the specifications of open-circuit voltage (V_{oc}) at 23.023 V, short-circuit current (I_{sc}) density at 2.9875 A/cm^2, and resulting fill factor of 0.733. The maximum V_{oc} and I_{sc} were 17.769 V and 2.5754 A/cm^2, respectively; consequently, the maximum power density was 45.763 W/cm^2. For determining the power of the TPV power system, an electric load device (331D; Prodigit, New Taipei City, Taiwan) was employed to evaluate the performance of the power output. The electric load was commanded using a computer equipped with GPID and RS232 via four modes, including constant voltage, constant resistance, constant power, and short circuit, detected five components. The electric load device revealed the corresponding information of current, voltage, and power. Here, the I–V curve is obtained by tuning diverse resistances between 0.5 Ω and 101.35 Ω, with the total selective resistance being 90 Ω.

2.3. Stirling engine

The Stirling engine played a crucial role in the current CHP system. The exhausted gas exiting from the downstream of the micro-combustor contained heat energy. In order to retrieve the waste heat of the exhausted gas, the external heat engine was situated on the top of the micro-combustor system. Therefore, the heat energy of the exhausted gas can be transformed into mechanical work, and hot water can be obtained because of the design of the engine-cooling system.

A small γ-type Stirling engine was designed in this study. Fig. 3 illustrates the layout and geometric parameters of the current Stirling engine, as well as the dimensions of the parameters shown in the right-hand table. This engine comprises two cylinders (power and a displacer cylinder), a displacer, and a power piston. The motions of the displacer and the power piston are governed by a crank that maintains a 90° phase angle between the displacer and the power piston. The power piston functions to deliver work produced by the engine, whereas the displacer shuttles working gas forwards and backward between hot and cold ends to facilitate the heat-transfer processes within the Stirling cycle. The engine's regenerator is housed inside the displacer, forming a so-called "moving regenerator" [47,48], which comprises several copper mesh layers stacked vertically to promote heat transfer between copper and working gas through efficient impingement heat transfer mechanism. This regenerator design eliminates the need to construct an additional regenerator chamber, making the engine more compact and easier to build. The engine is water-cooled. Fig. 4 shows the water tank at the cold end and illustrates the hot end's insulation shield which reduces heat loss to the ambient. As shown in Fig. 5, the cooling water is circulated between the cold-end water tank and an external water reservoir. The water reservoir is located slightly higher than the cold-end water tank; hence, the cooling water can be circulated naturally thought thermosiphon mechanism, and no extra power is needed to drive water circulation. The cooling water also serves to recycle some of the waste heat from the engine, increasing the overall energy efficiency even further.

The power generated by the Stirling engine is used to drive a DC generator, and the generated current and voltage are measured to calculate the electric power. The Stirling engine's power is then added to the power of the GaSb PV to determine the total power of the device.

3. Efficiency assessment

In this study, the CHP system comprised a GaSb PV cell array and a Stirling engine. Therefore, the power efficiency of the GaSb PV cell array and the Stirling engine must be determined individually to estimate the overall efficiency of the micro-CHP system. GaSb PV cell array was used to absorb the luminous light energy and generate electricity. The effective power efficiency (η_r) could be identified as the ratio of output electrical power to incident radiating power, and the overall efficiency with regard to GaSb PV cell array ($\eta_{t,PV}$) is determined as the ratio of output power generated by GaSb PV cell array to the heat-release rate of the fuels. In general, the heating values of CH_4, H_2, and CO were 36.408, 12.744, and 11.578 J/m^3, respectively.

$$\eta_r = \frac{Output\ electrical\ power}{Incident\ radiating\ power} \tag{1}$$

$$\eta_{t,PV} = \frac{Output\ power\ generated\ by\ PV\ cell}{Heat\ \ release\ rate\ of\ the\ fuels} \tag{2}$$

The Stirling engine can simultaneously yield electricity and hot water; thus, the overall generated energy can be categorized into two energy forms: heat and electricity. For the water heating system, the initial temperature of water filled in the water tank was

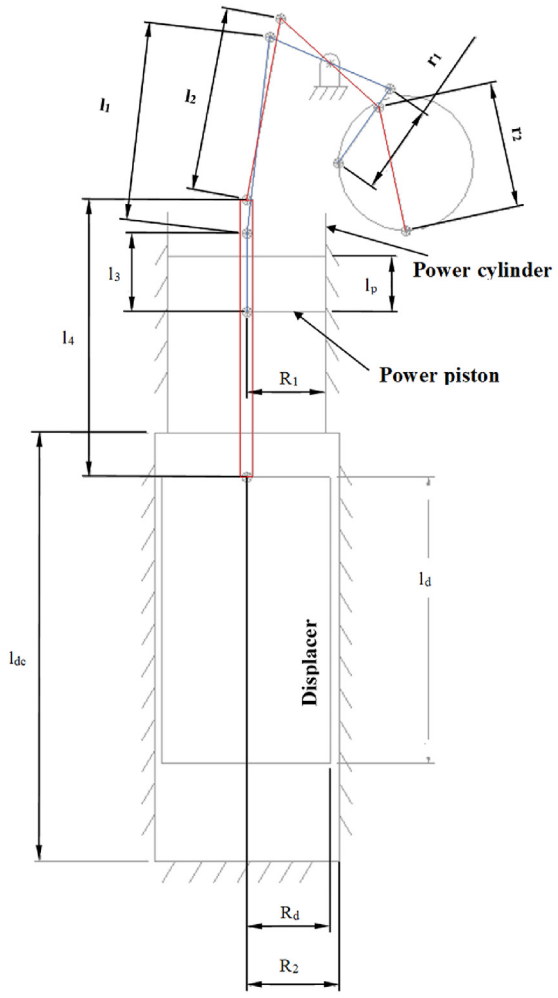

R_1 (m)	0.0250
R_2 (m)	0.0300
R_d (m)	0.0295
r_1 (m)	0.0250
r_2 (m)	0.0250
l_1 (m)	0.0796
l_2 (m)	0.0105
l_3 (m)	0.0850
l_4 (m)	0.0811
l_d (m)	0.0878
l_{dc} (m)	0.1400

Fig. 3. Layout and geometric parameters of the Stirling engine.

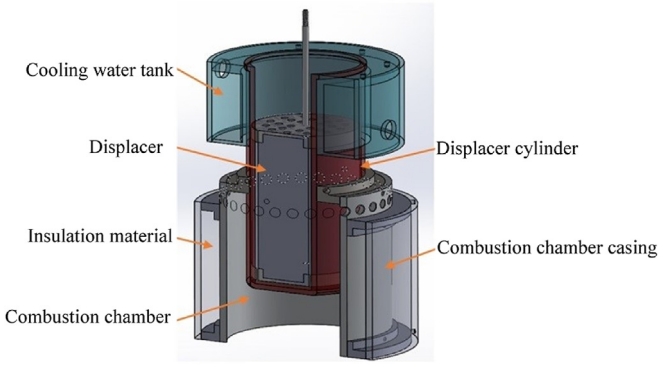

Fig. 4. Cooling tank and hot-end insulation shield.

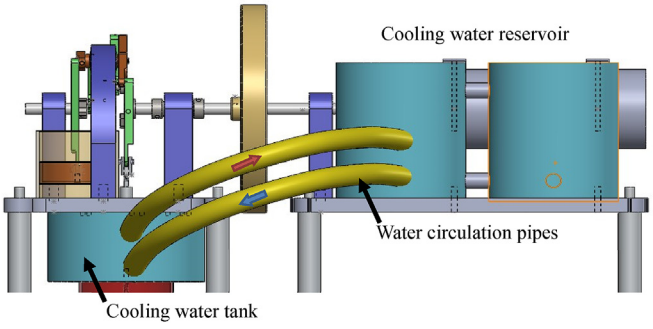

Fig. 5. Cooling water circulation.

295 K. The temperature of the water increased to 316 K when the entire system was operated for 10 min, as measured using a thermometer. The energy generated from the water tank in a steady stae condition can be defined by:

$$H = Mc\Delta T, \quad (3)$$

where H (in J) is the total energy obtained by water, M (in kg) is the total mass, c (in J/kg K) is the specific heat of water, and ΔT (in K) is the variation in the temperature of water between heated and initial conditions. The overall efficiency with regard to Stirling engine ($\eta_{t,SE}$) is designated as the ratio of output power generated by the combination of Stirling engine and power generator to heat release rate of the fuels.

$$\eta_{t,CHP} = \frac{Output\ power\ generated\ by\ Stirling\ engine - driven\ power\ system}{Heat\ release\ rate\ of\ the\ fuels} \quad (4)$$

To maximize the electrical output of the platinum micro-combustion system, the electric power efficiency (η_e), identified as the ratio of electricity generated by GaSb PV cells and Stirling engine-driven power system, is pivotal to evaluate the conversion rate of chemical to electrical energy. Finally, to assess the overall efficiency of the micro-CHP system fed by bio-syngas and natural gas, the overall efficiency ($\eta_{t,CHP}$) is designated as the ratio of heat and power output generated by the micro-CHP system to heat release rate provided by the fuels.

$$\eta_{t,CHP} = \frac{Heat\ and\ power\ output\ generated\ by\ micro - CHP\ system}{Heat\ release\ rate\ of\ the\ fuels} \quad (5)$$

$$\eta_{e} = \frac{Output\ power\ generated\ by\ PV\ cell\ and\ Stirling\ engine - driven\ power\ system}{Heat\ release\ rate\ of\ the\ fuels} \quad (6)$$

4. Results and discussion

4.1. Combustion characteristics

Derivative syngas from coal or biomass attracts numerous attention. The main components of syngas are carbon monoxide (CO) and hydrogen (H_2). The concentration ratios of CO and H_2 are usually 0.5–2 [49]. While the ratio of syngas constituents is different, combustion characteristics will be different, including flame speeds as well as flammability limits. For combustion, H_2 is critical to improving lean-flame stability and extending the flammability limit. Nevertheless, it shows some inherent disadvantages for syngas combustion, such as low calorific (BTU) value as well as low energy density, leading to narrow flammability limits, low flame temperature, and low combustion efficiencies. The literature [50,51] proves that catalytic combustion may efficiently improve the stability during the fuel-lean combustion, diminish exhausting pollution, and expand BTU flammability limits. Thus, the use of catalysts exhibits the potential for syngas-based fuel combustion that operates at low BTU conditions.

In addition, an intermittent supply and fuel variability of the bio-syngas mixture are an inevitable challenge in the development of a bio-syngas–fueled micro-CHP power system. Consequently, bio-syngas cofired with natural gas (i.e., methane) is a plausible fashion to tackle the aforementioned challenge. In this study, a CH_4–air mixture was used to mimic natural gas supply from the grid, and a stoichiometric CH_4–air mixture was delivered into the outer combustion chamber of the platinum micro-combustor with a fixed flow velocity of 5 m/s. Nevertheless, compared to H_2 and CO, CH_4 showed much lower reactivity and sticking coefficient on platinum. This implies that it is not easy to ignite CH_4 on platinum. In order to convert CH_4 completely, high wall temperature and large surface area of catalytic platinum were necessary. Hence, CH_4–air mixture was delivered into the outer chamber and combusted successfully, while the heat of the H_2/CO–air mixture in the inner chamber was released during combustion. The effects of fuel composition and equivalent ratio of the H_2/CO–air mixture on the inception of CH_4–air catalytic combustion were tested experimentally. Fig. 6 exhibits the photographies of the micro platinum combustion system during combustion under various inner equivalence ratios (ER_{in}) of the H_2/CO–air mixture with the given outer equivalence ratios of the CH_4–air mixture (ER_{out} = 1.0). Five fuel compositions of the H_2/CO–air mixture were compared: 90% H_2+10%CO, 70%H_2+30%CO, 50%H_2+50%CO, 30%H_2+70%CO and 10% H_2+90%CO, respectively. When ER_{in} = 0.6, the luminosities were orange in the middle and red in the end sections of the micro-combustor. The luminous light distribution was nonuniform. Although the luminosities of the micro-combustor slightly increased with an increase in CO content in the H_2/CO–air mixture, the luminous intensities for all the cases of ER_{in} = 0.6 were <12,000 W/m^2. When the fuel composition was 90%H_2+10%CO, the luminous light intensity of the micro-combustor was weak with an irradiance of 7204 W/m^2, but the resulting fuel conversion rates for H_2 and CH_4 measured using a gas analyzer indicated near completion. Essentially, the heat release from inner H_2/CO–air reaction seemed to induce sufficiently the catalytic combustion of outer CH_4; even the unburnt hydrocarbon fuel could be further consumed in post flames. When the fuel composition reached 50% H_2+50%CO and 10%H_2+90%CO, the luminosities of the micro-combustor apparently increased and became orange, with the corresponding irradiance reaching 9185 and 11,166 W/m^2, respectively. While ER_{in} increased to 0.8, the light irradiance of the micro-combustor increased and the luminous light transited from orange to bright yellow, with an increase in CO content in the H_2/CO–air mixture. The fuel conversion rates of H_2 and CH_4 in all cases were completed. In the case of 90%H_2+10%CO, the resulting irradiance of the micro-combustor is 19,127 W/m^2. Furthermore, in the cases of 50%H_2+50%CO and 10%H_2+90%CO, the micro-combustor achieved irradiance of 22,914 and 27,456 W/m^2, respectively. The thermal energy produced from the H_2/CO–air exothermic reaction surpassed the energy required that can sustain the catalytic combustion of outer methane. The luminous light became bright yellow, with a uniform luminous light distribution, leading to the corresponding irradiance exceeding 15,000 W/m^2 on average. When the ER_{in} increased to 1.0, the luminous intensity of the micro-combustor increased with increases in the CO content in the H_2/CO–air mixture, with the luminous light becoming bright white. The corresponding irradiance for all cases exceeded 30,000 W/m^2—for example, they are 41,978, 46,991, and 57,084 W/m^2 for 90% H_2+10%CO, 50%H_2+50%CO, and 90%H_2+10%CO, respectively. The heating value of H_2 was 12.744 J/m^3, larger than that of CO (11.578 J/m^3). The total heating value of the H_2/CO–air mixture may slightly

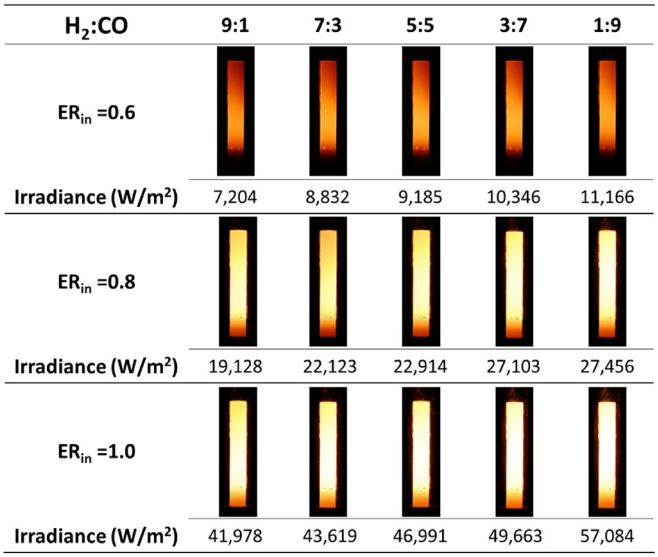

Fig. 6. Combustion of the micro-TPV reactor in various ER_{in} of the H_2/CO–air mixtures for five fuel composition ratios.

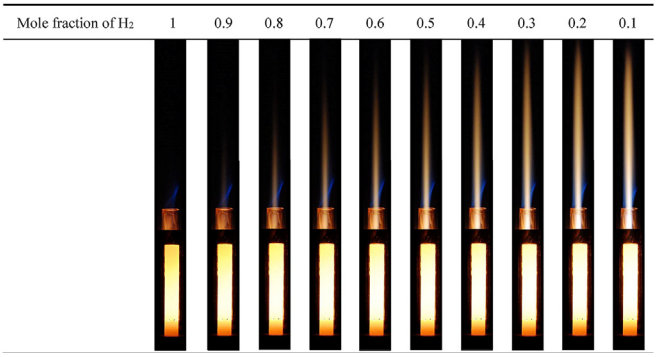

Fig. 8. Combustion of the micro-TPV reactor under various fuel composition of the H_2/CO–air mixture, with stoichiometric conditions for CH_4–air and H_2/CO–air mixtures.

decrease with an increase in the CO content in the H_2/CO–air mixture. However, it is entirely distinct for the characteristics of H_2 reaction on the catalyst surface and those of CO. H_2 has a tendency to react with catalytic bed and hence release heat earlier, whereas CO reacts later at the tail of the catalytic tube. Increasing CO concentration in the H_2/CO–air mixture may improve the dominance of homogeneous reaction in H_2/CO–air catalytic combustion, leading to the extension of the luminous region toward the downstream section of the micro-combustor.

From the irradiance, the luminous light intensities of the micro-combustor can be assorted into Levels 1 (<12,000 W/m^2), 2 (12,000–30,000 W/m^2), and 3 (>30,000 W/m^2). Theoretically, the luminous light intensities of Levels 1, 2, and 3 are advisable for converting light energy into electrical energy by using the TPV cell array. However, when the micro-combustor operates in Level 3, the micro-combustor probably runs with a tremendously high wall temperature, leading to the structural degradation of the platinum tube. Fig. 7 exhibits that the luminous emissions of the micro-TPV reactor are operated under various fuel compositions and flowrates of the H_2/CO–air mixture. The CH_4–air mixture for the outer chamber was fixed in a stoichiometric condition, whereas the H_2/CO–air mixture for the inner chamber operated with various equivalence ratios of 0.6, 0.8, and 1.0. Spanning from fuel-lean to stoichiometric conditions, the increase of flow velocity of the H_2/CO–air mixture may have increased fuel input, leading to an increase in the luminous light intensity of the micro-combustor. Moreover, the increase in the CO content in the H_2/CO–air mixture may increase the luminous light intensity of the micro-combustor. As shown in Fig. 7a, when ER_{in} of the H_2/CO–air mixture = 0.6, most luminous light intensities were <12,000 W/m^2, unless the total flow velocity of the H_2/CO–air mixture or carbon monoxide content in the H_2/CO–air mixture increased, in which case, the luminous light intensity of the micro-combustor increased to Level 2 (>12,000 W/m^2). As shown in Fig. 7b and c, the equivalence ratios of the H_2/CO–air mixture were 0.8 and 1.0 and the operational ranges for the two conditions were similar. A flow velocity of the H_2/CO–air mixture ≤3 m/s was potentially inappropriate for power generation by using a TPV cell array due to the low luminous light intensity of the micro-combustor. By contrast, the H_2/CO–air mixture with a flow velocity above 6 m/s may be dangerous to the micro-combustor because of the wall temperature exceeding the temperature tolerance of platinum material. Thus, when the equivalence ratio of the H_2/CO–air mixture is 0.8–1.0, the

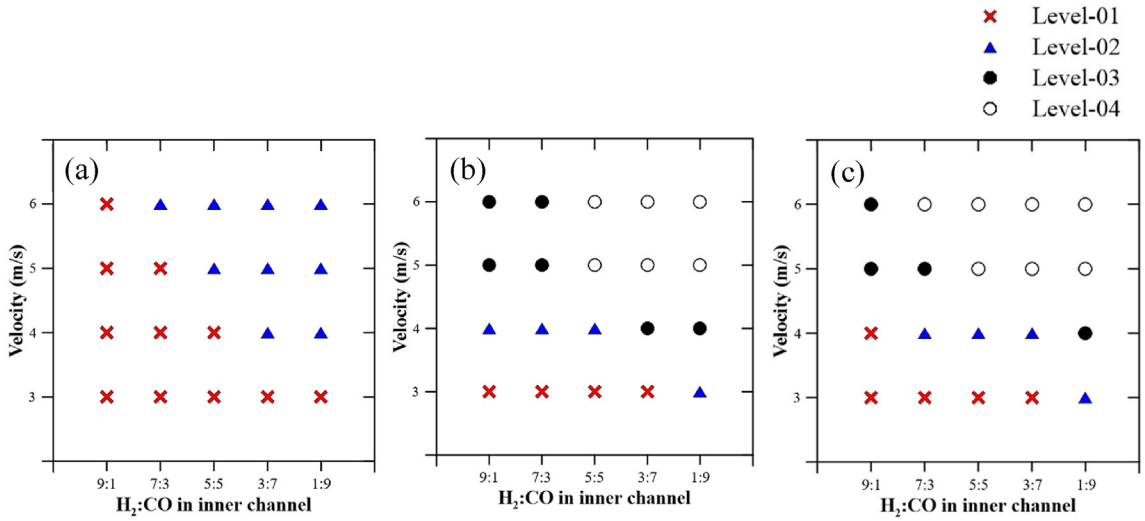

Fig. 7. Different range of luminous emissions of the micro-combustors under various fuel compositions and flowrates of the H_2/CO–air mixture; ER_{out} = (a) 0.6, (b) 0.8, and (c) 1.0.

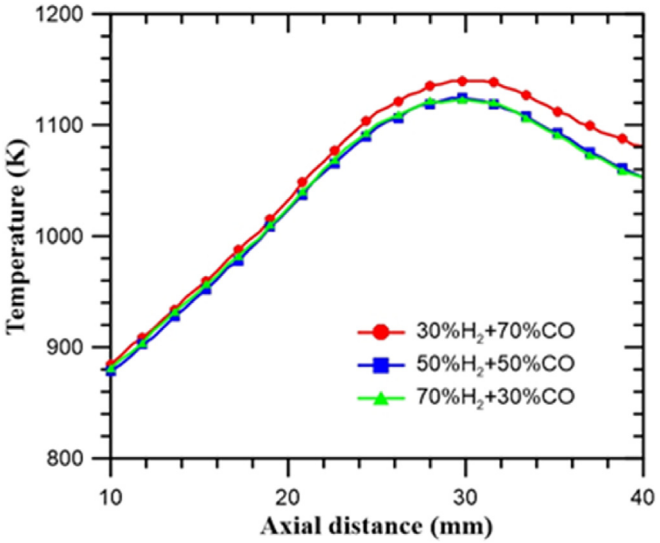

Fig. 9. Surface temperature distribution along the micro-TPV under various fuel composition of the H_2/CO–air mixture, with stoichiometric conditions for CH_4–air and H_2/CO–air mixtures.

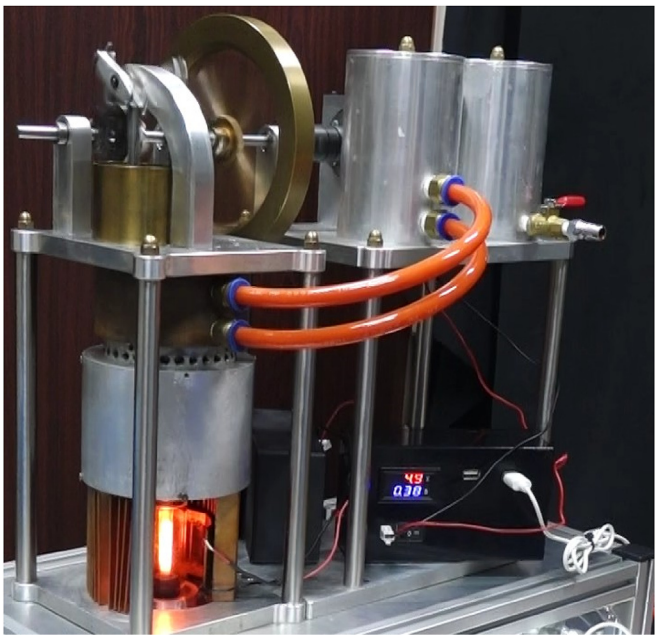

Fig. 10. Micro-CHP system assembled with a TPV cell array, Stirling engine, and power generator.

fuel composition of the H_2/CO–air mixture is irrelevant to the luminous irradiation of the micro-combustor.

In order to determine the combustion efficiency, five fuel composition conditions were selected for further estimation: 90%H_2+10%CO, 70%H_2+30%CO, 50%H_2+50%CO, 30%H_2+70%CO, and 10%H_2+90%CO for the micro-TPV reactor; these were with consistent $ER_{in,\ CH4} = ER_{out,\ H2/CO} = 1.0$ and flow velocity = 5 m/s. Fig. 8 illustrates combustion in the micro-TPV reactor under five conditions. Except for the luminous feature on the micro-combustor, there was post-flame tailing from the inner and outer chambers of the micro-combustor. In the case of 0.9 mol fraction of H_2 (90%H_2+10%CO), it had a blue annular flame anchored on the outer chamber and a jet flame tailing from the inner chamber. Thus, the catalytic combustion of the H_2/CO–air, and CH_4–air mixtures can be sustained in the micro-combustor in these five conditions. As the CO content in the H_2/CO–air mixture increases, the jet flame tailing from the inner chamber becomes significant and intense. Unburned carbon monoxide may further react in the downstream jet flame. Furthermore, the tail flame color changed to bright white because of the increase in the CO content in the H_2/CO–air mixture; thus, increasing CO content attributes the dominant transition of catalytic combustion from a heterogeneous to a homogeneous reaction. The surface temperature distribution for three conditions was shown in Fig. 9, and the maximal surface temperatures obtained by the infrared thermal imaging camera were approximately 1200 K, concentrated in section 20–35 cm away from the base of the micro-combustor. With an increase in the CO content in the H_2/CO–air mixture, the surface temperature increased, and the maximum temperature distribution moved towards the downstream section of the micro-combustor. Besides, the residual CH_4 and H_2 content in the exhausted gas was obtained using the gas analyzer to evaluate the consequences of catalytic combustion; therefore, the conversion rate of fuel could be defined. The hydrogen and methane converted completely since H_2 and CH_4 were not detected in the exhausted gas. Based on the results of the previous studies [33,38], H_2 is prone to react on the catalyst, facilitating the subsequent CO catalytic combustion. Additionally, methane may flow through the perforated holes to the outer chamber and further induce the catalytic gas-phase reaction in the presence of the inward-diffused radicals from H_2/CO–air mixture reaction. The exothermic heat derived from the induced catalytic gas-phase reaction leads to a high surface temperature of the micro-combustor, and the complete fuel conversion for the CH_4–air and H_2/CO–air mixtures can be achieved. The improved combustion strength eventually promotes that the irradiance of the TPV combustor increases and provides high flue temperature for the Stirling engine-driven power system. In addition, the platinum tubular reactor is qualified to overcome the fuel variability from bio-syngas supply system and provide stable combustion for the micro-CHP power system.

4.2. Demonstration of micro-CHP power system

In this study, the bio-syngas combustion–driven micro-CHP system was prototyped as shown in Fig. 10. A GaSb PV cell array, placed around the micro-combustor, was implemented to convert the radiant energy from the micro-combustor to electricity. The Stirling engine, placed on the top of the micro-combustor, was engaged to convert the thermal energy of flue gas to electricity by using a generator and store thermal energy in a water tank. The micro-CHP system apparently functioned stably and reliably under various bio-syngas fuel supply conditions. The repeatability and maneuverability of the micro-CHP system were also considerable.

This section describes the operation of the micro-CHP system stoichiometric CH_4–air and H_2/CO–air conditions, but there are only three H_2/CO fuel compositions, 70%H_2+30%CO, 50%H_2+50%CO, and 30%H_2+70%CO.

First, to assess the contribution of electric power generation in the GaSb TPV cell array, measuring the power output of radiation

Table 1
Measured radiation intensity for the micro-combustor.

H_2:CO	70%:30%	50%:50%	30%:70%
Irradiation (W/m^2)	43,619	46,991	49,663
Radiation energy (W)	32.89	35.43	37.45
Input energy (W)	785.06	777.44	769.83
Effective power efficiency (η_r, %)	4.19	4.55	4.86

Table 2
Various TPV electrical output for the micro-combustor.

H_2:CO	70%:30%	50%:50%	30%::70%
TPV cell array			
Max. actual power output (W)	3.2	3.5	4.1
Overall efficiency ($\eta_{t,PV}$, %)	0.41	0.45	0.53
Stirling engine with power generator			
Power output (W)	2.45	2.70	2.76
Overall efficiency ($\eta_{t,SE}$, %)	0.31	0.35	0.36
Micro CHP system			
Electric power efficiency (η_e)	0.52	0.58	0.63
Water temperature (°C)	25	26	29
Energy gained by water (W)	261.6	272.1	303.5
Overall efficiency ($\eta_{t,CHP}$, %)	33.3	35.0	39.4

from the micro-combustor is necessary. Therefore, the micro-combustor was situated in the center of the integrating sphere to evaluate the light radiation generated from the emission of combustor. An optical fiber was also employed to deliver the radiation to a spectral meter for measuring the irradiance. With multiplying the irradiance and surface area of the combustor (7.54×10^{-4} m^2), the power output of radiation can be determined subsequently. The actual conversion of fuels was also evaluated by the energy input of fuels. Therefore, Table 1 presents the results of irradiation and radiation efficiency of the micro-combustor for 70% H_2+30%CO, 50%H_2+50%CO, and 30%H_2+70%CO, all with the given velocity of 5 m/s and stoichiometric condition for the CH_4–air and H_2/CO–air mixtures. The irradiance for 70%H_2+30%CO, 50%H_2+50% CO, and 30%H_2+70%CO was 43,619, 46,991, and 49,663 W/m^2, respectively. Multiplying with the effective surface area of the micro-combustor, the resulting radiation energy was 32.89, 35.43, and 37.45 W for 70%H_2+30%CO, 50%H_2+50%CO, and 30%H_2+70% CO, respectively. Consequently, the η_r (the ratio of output power to radiation power) was 4.19%, 4.55%, and 4.86% for 70%H_2+30%CO, 50%H_2+50%CO, and 30%H_2+70%CO, respectively.

Table 2 lists the experimental results of the electrical output generated by the TPV cell array system and its corresponding overall efficiency with regard to the TPV cell array ($\eta_{t,PV}$)—defined as the ratio of output power generated by TPV cells to the heat release rate of the fuels. Under the condition of 70%H_2+30%CO, the power output was 3.2 W, corresponding to an overall efficiency ($\eta_{t,PV}$) of 0.41%. When the CO content increased, the power output ($\eta_{t,PV}$) under 50%H_2+50%CO and 30%H_2+70%CO improved to 3.5 W (0.45%) and 4.1 W (0.53%), respectively. Thus, the overall efficiency with regard to the TPV cell array was proportional to the irradiance intensity and luminous uniformity of the micro-combustor; in other words, increasing CO content in the H_2/CO mixture contributed toward the enhancement of the $\eta_{t,PV}$.

Regarding the power output of the Stirling engine with the power generator, the electrical output was 2.45, 2.70, and 2.76 W for 70%H_2+30%CO, 50%H_2+50%CO, and 30%H_2+70%CO, respectively. The overall efficiency with regard to the Stirling engine ($\eta_{t,SE}$) is designated as the ratio of output power generated by the combination of Stirling engine and power generator to heat release rate of the fuels; the resulting $\eta_{t,SE}$ was 0.31%, 0.35%, and 0.37% for 70% H_2+30%CO, 50%H_2+50%CO, and 30%H_2+70%CO, respectively. However, the η_e of the micro-CHP system—the ratio of electricity generated by the TPV cell array and Stirling engine–driven power system—is 0.52%, 0.56%, and 0.63% for 70%H_2+30%CO, 50%H_2+50% CO, and 30%H_2+70%CO, respectively.

For measuring the thermal energy of heating water, the micro-CHP system was operated for 10 min, and then, the water temperature in the water tank was measured. As listed in Table 2, the destination water temperatures were 25 °C, 26 °C, and 29 °C for 70% H_2+30%CO, 50%H_2+50%CO, and 30%H_2+70%CO, respectively. The thermal energy gained by water was 261.6, 272.1, and 303.5 W for 70%H_2+30%CO, 50%H_2+50%CO, and 30%H_2+70%CO, respectively. The overall efficiency ($\eta_{t,CHP}$), designated as the ratio of heat and power output generated by the micro-CHP system to heat release rate of the fuels, is 33.3%, 35.0%, and 39.4% for 70%H_2+30%CO, 50% H_2+50%CO, and 30%H_2+70%CO, respectively. Although its overall efficiency was less than 40%, the feasibility and maneuverability of the bio-syngas combustion-driven micro-CHP system with a platinum tubular combustor were high. Primary thermal energy retains in the flue gas. The overall efficiency improvement of bio-syngas combustion-driven micro-CHP system can be realized by optimizing the thermal management of this proposed system, achieving to increase systematic efficiencies individually.

5. Conclusion

To mitigate fuel variability and supply intermittency to biomass-based combustion–driven power systems, a platinum tube with perforated holes was used in the micro-CHP system and cofired with natural gas. A methane-air mixture was considered the natural gas and delivered into the outer chamber of the micro-combustor, whereas an H_2/CO-air mixture with various fuel compositions was simulated as bio-syngas and delivered to the inner chamber of the micro-combustor. The combustion characteristics and operating envelope of the micro-combustor were analyzed systematically. By fabricating the micro-combustor within a TPV cell array and a Stirling engine, the effective power efficiency and overall efficiency of the micro-CHP power system were evaluated under different fuel compositions. The feasibility and maneuverability of bio-syngas combustion–driven micro-CHP system with a platinum tubular combustor were thus demonstrated. Some highlights are shown below:

1. H_2 is prone to react on the catalyst and facilitate the subsequent CO catalytic combustion. CH_4 may flow through the perforated holes to the outer chamber and induced a catalytic gas-phase reaction in the presence of inward-diffused radicals from the H_2/CO–air mixture reaction. The exothermic heat of the induced catalytic gas-phase reaction leads to the high surface temperature of the micro-combustor and achieves complete fuel conversion for the CH_4–air and H_2/CO–air mixtures.
2. The prototype of micro-combustion integrated with a TPV cell array and a Stirling engine was tested with various fuel compositions. The micro-CHP system is apparently stable and reliable for various bio-syngas fuel supply conditions. The repeatability and maneuverability of the micro-CHP system are also considerable.
3. The η_e of the micro-CHP system considered the ratio of electricity generated by the TPV cell array and Stirling engine-driven power system, is 0.52%, 0.58%, and 0.63% for 70%H_2+30%CO, 50% H_2+50%CO, and 30%H_2+70%CO, respectively. When the thermal energy of the heating water is considered, the overall efficiency ($\eta_{t,CHP}$) increases to 33.3%, 35.0%, and 39.4% for 70%H_2+30%CO, 50%H_2+50%CO, and 30%H_2+70%CO, respectively. Despite verifying the concept of bio-syngas combustion–driven micro-CHP, optimizing the component performance of micro-CHP system remains a priority.

Declaration of competing interest

All authors declared that: (i) no support, financial or otherwise, has been received from any organization that may have an interest in the submitted work; and (ii) there are no other relationships or activities that could appear to have influenced the submitted work.

Acknowledgments

The authors thank the financial support from the Ministry of Science and Technology, Taiwan under the grant numbers, MOST 106-2923-E-006-003-MY3, MOST 106-3113-E-006-002-CC2, and MOST 108-2628-E-006-008-MY3.

References

[1] Ozawa A, Kudoh Y. Performance of residential fuel-cell-combined heat and power systems for various household types in Japan. Int J Hydrogen Energy 2018;43(32):15412–22.
[2] Barelli L, Bidini G, Gallorini F, Ottaviano A. Dynamic analysis of PEMFC-based CHP systems for domestic application. Appl Energy 2012;91(1):13–28.
[3] Wang Y, Chen KS, Mishler J, Cho SC, Adroher XC. A review of polymer electrolyte membrane fuel cells: technology, applications, and needs on fundamental research. Appl Energy 2011;88(4):981–1007.
[4] Dentice d'Accadia M, Sasso M, Sibilio S, Vanoli L. Micro-combined heat and power in residential and light commercial applications. Appl Therm Eng 2003;23(10):1247–59.
[5] Pepermans G, Driesen J, Haeseldonckx D, Belmans R, D'haeseleer W. Distributed generation: definition, benefits and issues. Energy Policy 2005;33(6):787–98.
[6] González A, Riba J-R, Rius A. Combined heat and power design based on environmental and cost criteria. Energy 2016;116:922–32.
[7] Bianchi M, De Pascale A, Spina PR. Guidelines for residential micro-CHP systems design. Appl Energy 2012;97:673–85.
[8] Buragohain B, Mahanta P, Moholkar VS. Biomass gasification for decentralized power generation: the Indian perspective. Renew Sustain Energy Rev 2010;14(1):73–92.
[9] Dornburg V, Faaij APC. Efficiency and economy of wood-fired biomass energy systems in relation to scale regarding heat and power generation using combustion and gasification technologies. Biomass Bioenergy 2001;21(2):91–108.
[10] Caputo AC, Palumbo M, Pelagagge PM, Scacchia F. Economics of biomass energy utilization in combustion and gasification plants: effects of logistic variables. Biomass Bioenergy 2005;28(1):35–51.
[11] Dong L, Liu H, Riffat S. Development of small-scale and micro-scale biomass-fuelled CHP systems – a literature review. Appl Therm Eng 2009;29(11):2119–26.
[12] Patuzzi F, Prando D, Vakalis S, Rizzo AM, Chiaramonti D, Tirler W, et al. Small-scale biomass gasification CHP systems: comparative performance assessment and monitoring experiences in South Tyrol (Italy). Energy 2016;112:285–93.
[13] Montuori L, Alcázar-Ortega M, Álvarez-Bel C, Domijan A. Integration of renewable energy in microgrids coordinated with demand response resources: economic evaluation of a biomass gasification plant by Homer Simulator. Appl Energy 2014;132:15–22.
[14] Ho WS, Hashim H, Lim JS. Integrated biomass and solar town concept for a smart eco-village in Iskandar Malaysia (IM). Renew Energy 2014;69:190–201.
[15] Zabaniotou AA, Skoulou VK, Mertzis DP, Koufodimos GS, Samaras ZC. Mobile gasification units for sustainable electricity production in rural areas: the SMARt-CHP project. Ind Eng Chem Res 2011;50(2):602–8.
[16] Farhad S, Hamdullahpur F, Yoo Y. Performance evaluation of different configurations of biogas-fuelled SOFC micro-CHP systems for residential applications. Int J Hydrogen Energy 2010;35(8):3758–68.
[17] Zeng H, Wang Y, Shi Y, Cai N. Biogas-fueled flame fuel cell for micro-combined heat and power system. Energy Convers Manag 2017;148:701–7.
[18] Chen XP, Wang YD, Yu HD, Wu DW, Li Y, Roskilly AP. A domestic CHP system with hybrid electrical energy storage. Energy Build 2012;55:361–8.
[19] Chen XP, Hewitt N, Li ZT, Wu QM, Yuan X, Roskilly T. Dynamic programming for optimal operation of a biofuel micro CHP-HES system. Appl Energy 2017;208:132–41.
[20] Lee U, Balu E, Chung JN. An experimental evaluation of an integrated biomass gasification and power generation system for distributed power applications. Appl Energy 2013;101:699–708.
[21] Li Y-H, Chen H-H. Analysis of syngas production rate in empty fruit bunch steam gasification with varying control factors. Int J Hydrogen Energy 2018;43(2):667–75.
[22] Kopczyński M, Lasek JA, Iluk A, Zuwała J. The co-combustion of hard coal with raw and torrefied biomasses (willow (Salix viminalis), olive oil residue and waste wood from furniture manufacturing). Energy 2017;140:1316–25.
[23] Heidenreich S, Foscolo PU. New concepts in biomass gasification. Prog Energy Combust Sci 2015;46:72–95.
[24] Pala LPR, Wang Q, Kolb G, Hessel V. Steam gasification of biomass with subsequent syngas adjustment using shift reaction for syngas production: an Aspen Plus model. Renew Energy 2017;101:484–92.
[25] Kohsri S, Meechai A, Prapainainar C, Narataruksa P, Hunpinyo P, Sin G. Design and preliminary operation of a hybrid syngas/solar PV/battery power system for off-grid applications: a case study in Thailand. Chem Eng Res Des 2018;131:346–61.
[26] Oh G, Ra HW, Yoon SM, Mun TY, Seo MW, Lee J-G, et al. Syngas production through gasification of coal water mixture and power generation on dual-fuel diesel engine. J Energy Inst 2019;92(2):265–74.
[27] Forman C, Gootz M, Wolfersdorf C, Meyer B. Coupling power generation with syngas-based chemical synthesis. Appl Energy 2017;198:180–91.
[28] Safer K, Ouadha A, Tabet F. Entropy generation in turbulent syngas counterflow diffusion flames. Int J Hydrogen Energy 2017;42(49):29532–44.
[29] Neto AFG, Marques FC, Amador AT, Ferreira ADS, Neto AMJC. DFT and canonical ensemble investigations on the thermodynamic properties of Syngas and natural gas/Syngas mixtures. Renew Energy 2019;130:495–509.
[30] Li Y-H, Lin H-T, Xiao K-L, Lasek J. Combustion behavior of coal pellets blended with Miscanthus biochar. Energy 2018;163:180–90.
[31] Yang SI, Wu MS, Wu CY. Application of biomass fast pyrolysis part I: pyrolysis characteristics and products. Energy 2014;66:162–71.
[32] Wu Y-T, Li Y-H. Combustion characteristics of a micro segment platinum tubular reactor with a gap. Chem Eng J 2016;304:485–92.
[33] Li Y-H, Chen G-B, Wu F-H, Cheng T-S, Chao Y-C. Combustion characteristics in a small-scale reactor with catalyst segmentation and cavities. Proc Combust Inst 2013;34(2):2253–9.
[34] Chen J, Gao X, Xu D. Kinetic effects of hydrogen addition on the catalytic self-ignition of methane over platinum in micro-channels. Chem Eng J 2016;284:1028–34.
[35] Deutschmann O, Maier LI, Riedel U, Stroemman AH, Dibble RW. Hydrogen assisted catalytic combustion of methane on platinum. Catal Today 2000;59(1–2):141–50.
[36] Karbasi M, Wierzba I. The effects of hydrogen addition on the stability limits of methane jet diffusion flames. Int J Hydrogen Energy 1998;23(2):123–9.
[37] Schefer RW, Wicksall DM, Agrawal AK. Combustion of hydrogen-enriched methane in a lean premixed swirl-stabilized burner. Proc Combust Inst 2002;29(1):843–51.
[38] Li Y-H, Chen G-B, Wu F-H, Cheng T-S, Chao Y-C. Effects of catalyst segmentation with cavities on combustion enhancement of blended fuels in a micro channel. Combust Flame 2012;159(4):1644–51.
[39] Zheng X, Mantzaras J, Bombach R. Kinetic interactions between hydrogen and carbon monoxide oxidation over platinum. Combust Flame 2014;161(1):332–46.
[40] Zheng X, Schultze M, Mantzaras J, Bombach R. Effects of hydrogen addition on the catalytic oxidation of carbon monoxide over platinum at power generation relevant temperatures. Proc Combust Inst 2013;34(2):3343–50.
[41] Yang WM, Chou SK, Shu C, Li ZW, Xue H. Development of micro-thermophotovoltaic system. Appl Phys Lett 2002;81(27):5255–7.
[42] Nielsen OM, Arana LR, Baertsch CD, Jensen KF, Schmidt MA. A thermophotovoltaic micro-generator for portable power applications. In: Conference A thermophotovoltaic micro-generator for portable power applications, vol. 1. IEEE; 2003. p. 714–7.
[43] Li YH, Li HY, Dunn-Rankin D, Chao YC. Enhancing thermal, electrical efficiencies of a miniature combustion-driven thermophotovoltaic system. Prog Photovoltaics 2009;17(7):502–12.
[44] Li YH, Lien YS, Chao YC, Dunn-Rankin D. Performance of a mesoscale liquid fuel-film combustion-driven TPV power system. Prog Photovoltaics 2009;17(5):327–36.
[45] Li Y-H, Hong J-R. Performance assessment of catalytic combustion-driven thermophotovoltaic platinum tubular reactor. Appl Energy 2018;211:843–53.
[46] Dry ME. The fischer–tropsch process: 1950–2000. Catal Today 2002;71(3–4):227–41.
[47] Li Y-H, Yang Y-C, Chen W-L. A parametric study on the effects of displacer-cylinder-circumferential-wall thermal conditions on the performance of a γ-type LTD Stirling engine. Int J Ambient Energy 2018:1–12.
[48] Chen W-L, Yang Y-C, Salazar JL. A CFD parametric study on the performance of a low-temperature-differential γ-type Stirling engine. Energy Convers Manag 2015;106:635–43.
[49] Li Y-H, Hsu H-W, Lien Y-S, Chao Y-C. Design of a novel hydrogen–syngas catalytic mesh combustor. Int J Hydrogen Energy 2009;34(19):8322–8.
[50] Alavandi SK, Agrawal AK. Experimental study of combustion of hydrogen-syngas/methane fuel mixtures in a porous burner. Int J Hydrogen Energy 2008;33(4):1407–15.
[51] Landong L, Jixin C, Shujuan Z, Fuxiang Z, Naijia G, Tianyou W, et al. Selective catalytic reduction of nitrogen oxides from exhaust of lean burn engine over in-situ synthesized Cu–ZSM-5/Cordierite. Environ Sci Technol 2005;39(8):2841–7.